

Photocatalytic Activity of Vanadium-Substituted ETS-10

Michael J. Nash,[†] Sergey Rykov,[†] Raul F. Lobo,^{*,†} Douglas J. Doren,[‡] and Israel Wachs[§]

Department of Chemical Engineering, University of Delaware, Newark, Delaware 19716, Department of Chemistry and Biochemistry, University of Delaware, Newark, Delaware 19716, and Operando Molecular Spectroscopy and Catalysis Lab, Chemical Engineering Department, LeHigh University, Bethlehem, Pennsylvania 18015

Received: November 3, 2006; In Final Form: March 7, 2007

Various amounts of vanadium have been isomorphously substituted for titanium in ETS-10, creating samples with V/(V+Ti) ratios of 0.13, 0.33, 0.43, and 1.00 and characterized experimentally using Raman, near-edge X-ray absorption fine structure (NEXAFS), X-ray powder diffraction, N₂ adsorption, scanning electron microscopy (SEM), UV/vis spectroscopy, and diffuse reflectance infrared Fourier transform spectroscopy (DRIFTS). Raman spectra reveal a disordered chain structure that contains different V–O bonds along with the presence of a V–O–Ti peak. The UV/vis spectra of the vanadium samples have three new absorption features in the visible region at 450, 594, and 850 nm, suggesting both V⁴⁺ and V⁵⁺ are present in the samples. NEXAFS results confirm the presence of both V⁵⁺ and V⁴⁺ in the vanadium samples, with a fraction of V⁴⁺ within the range of 0.2–0.4. The addition of vanadium lowers the band gap energy of ETS-10 from 4.32 eV to a minimum of 3.58 eV for the 0.43ETVS-10 sample. Studies of the photocatalytic polymerization of ethylene show that the 594 nm transition has no photocatalytic activity. The visible transition around 450 nm in the vanadium-incorporated samples is photocatalytically active, and the lower-concentration vanadium samples have higher photocatalytic activity than that of ETS-10 and AM-6, the all-vanadium analogue of ETS-10.

1. Introduction

ETS-10 is a unique microporous titanosilicate invented in 1989 by Kuznicki.¹ It is composed of octahedrally coordinated TiO_{6/2} units and tetrahedrally coordinated SiO_{4/2} units. These TiO_{6/2} corner-sharing octahedra connect through the apical oxygen atoms, forming linear chains which are surrounded by corner-sharing SiO_{4/2} tetrahedra. The linear chains form a three-dimensional 12-ring pore structure, with an ideal unit cell composition of (Na,K)₂TiSi₅O₁₃.² The structure of ETS-10 is inherently disordered and can be described as an intergrowth of two polymorphs. Figure 1 depicts the structure of one of these polymorphs as well as an enlarged section of the chain and its surface termination.

The unique structure of ETS-10 has motivated much research to determine its viability in applications such as membrane separations,³ acid–base catalysis,^{4,5} photocatalysis,⁶ and shape-selective photocatalysis.^{7,8} In photocatalytic applications, the titanium chains of ETS-10 act as semiconductor “quantum wires”. Electron–hole pairs are created when ETS-10 is exposed to radiation greater than its band gap energy of 4.03 eV.⁹ These electron–hole pairs can travel down the chain where they can initiate reactions with molecules at the termination of the chains or at structural defects along the chains.⁶ Krisnandi et al.⁶ have shown that the selectivity of ETS-10 samples is dependent on the number of defects, with defective samples causing the complete oxidation of ethylene, as opposed to the partial oxidation observed on defect-free samples. Xamena et al.⁷ have shown that a postsynthesis treatment with dilute HF creates

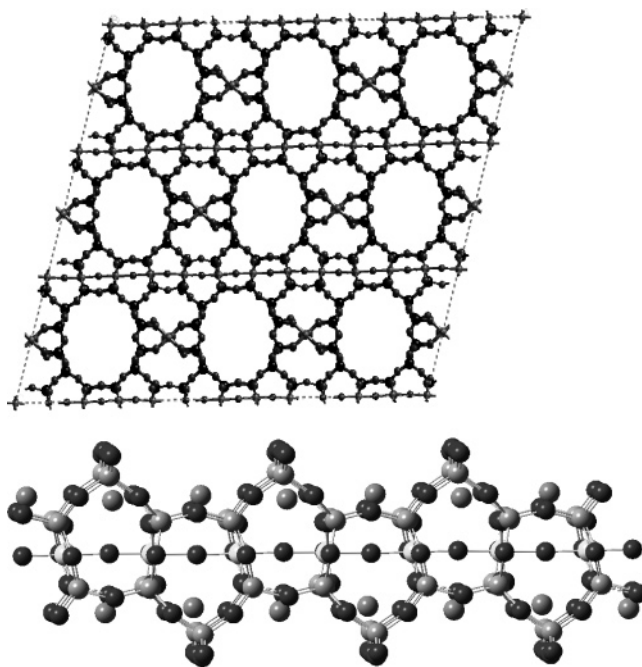


Figure 1. Polymorph B and an enlarged section of the titanium chain of ETS-10 with SiO_{4/2} tetrahedra and Na cations surrounding the TiO_{6/2} units.

defects in ETS-10 and increases the reactivity of the samples in the photodegradation of large aromatic compounds.

Formation of electron–hole pairs is one of the key steps in the photodegradation of volatile organic compounds (VOCs), and current research is aimed at discovering photocatalysts with band gaps in the visible range without decreasing the oxidation potential of the holes.¹⁰ One approach is to isomorphously

* To whom correspondence should be addressed. Tel: 302 831 1261. Fax: 302 831 2085. E-mail: lobo@udel.edu.

[†] Department of Chemical Engineering, University of Delaware.

[‡] Department of Chemistry and Biochemistry, University of Delaware.

[§] LeHigh University.

substitute Ti with other transition metals such as Cr,¹¹ Fe,¹² and V.^{13,14} In the case of V, Ti can be completely replaced, forming a material known as AM-6.¹³ However, little research has been conducted on the photocatalytic properties of these transition-metal-substituted forms of ETS-10. Uma et al.¹⁵ studied the photocatalytic properties of chromium- and cobalt-substituted ETS-10 in the decomposition of acetaldehyde, though Co is believed to be substituting for Si rather than Ti. They found that these materials were active photocatalysts in the visible region only after calcination of the samples at 500 °C. They attribute this to the formation of higher oxidation states of Cr and Co upon calcination. Here, we investigate the photocatalytic properties of vanadium-substituted ETS-10 (ETVS-10) and compare the results to ETS-10 and titania P-25. We begin by first describing the synthesis procedure used to create these materials followed by a detailed description of the experimental methods used to characterize them. Next, we present the characterization and the photocatalytic properties of the materials, followed by a discussion of the results, and finally concluding with a brief summary of the important results. These results show that the vanadium-incorporated samples have the vanadium substituted for the titanium with a mixture of V⁵⁺ and V⁴⁺. These results also show that the vanadium-incorporated samples have increased photocatalytic activity in the visible region of the spectrum, with the mixed samples showing the highest reactivity.

2. Experimental Methods

2.1. Synthesis. The synthesis of the ETS-10 samples was carried out according to the protocol of Lv et al.¹⁶ in which a gel solution with a molar ratio of 3.4 Na₂O/1.5 K₂O/TiO₂/5.5 SiO₂/160 H₂O was sealed in a Teflon-lined autoclave (Parr 23 mL) and heated at 230 °C for 3 days. The crystalline product was then vacuum filtered, washed with DI water, and dried at room temperature.

For vanadium-incorporated samples, various amounts of VOSO₄·5H₂O (Aldrich) were added to the parent gel to form ETVS-10 samples with different V/(V+Ti) molar ratios. To identify these samples, a naming convention of V/(V+Ti)ETVS-10 was used, where a ratio value of 0 corresponds to ETS-10 and a value of 1 to AM-6. The ratio V/(V+Ti) was that used in the synthesis mixture, which turned out to be very similar to the ratio in the solid, as verified by EDAX. Thus, in the synthesis of 0.33ETVS-10 (V/(V+Ti) = 0.33), two solutions were prepared and were then mixed to form the synthesis gel, one containing 11.13 g of sodium silicate (14% NaOH, 27% SiO₂, Aldrich), 2.24 g of KCl, 1.70 g of NaCl, and 7.42 g of DI water and the other containing 14.85 g of DI water, 0.80 g of P-25 (Degussa), and 1.27 g of VOSO₄·5H₂O (Aldrich). Once these two solutions were mixed, the pH was adjusted to approximately 10.4, using NaOH or HCl (concentrated Aldrich), before sealing in the autoclave. Samples with molar ratios of 0.13, 0.33, and 0.43 were prepared for this investigation. The synthesis of AM-6 was carried out following the protocol of Rocha et al.¹³ at 185 instead of 230 °C.

2.2. Characterization. Powder X-ray diffraction (XRD) data were collected on a Philips X'pert diffractometer using a Cu K α source. The patterns were obtained from 5 to 50° 2 θ using a step size of 0.02° 2 θ and 2 s per step. Adsorption isotherms were collected on a Micromeritics ASAP 2010 using N₂ as the adsorbate. SEM images and EDAX analysis were obtained on a JEOL JSM7400F microscope at 30000 \times magnification. UV-vis spectra were obtained on a Jasco V-550 spectrometer equipped with an ISV-469 integrating sphere from 850 to 200

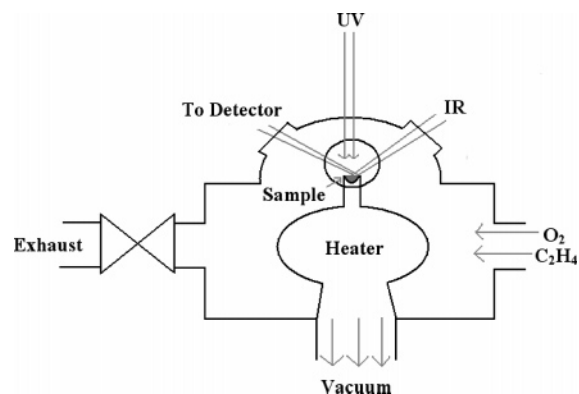


Figure 2. DRIFTS cell setup. The O₂ and C₂H₄ enter the chamber from the feed port and then travel through the sample to the vacuum pumps. IR radiation enters the chamber through the right KBr window, reflects off the sample, and exits through the left KBr window, while UV enters through the center SiO₂ window.

nm with a bandwidth of 1 nm and using MgO as a reference material. The ambient Raman spectra were collected in ambient air using a diode laser (Coherent Verdi, 532.050 nm) with an exposure time of 3 s and an accumulation time of 4 s. The in situ Raman spectra were collected with a visible laser excitation of 532 nm (20 mW, YAG laser) in the 100–1200 cm⁻¹ region on a combined UV/visible Raman spectrometer system (Horiba–Jobin Yvon LabRam-HR) equipped with a confocal microscope (Olympus BX-30), notch filter (532 nm), and a single-stage monochromator (Horiba–Jobin Yvon LabRam-HR), with a 900 grooves/mm grating. The laser power at the sample was kept below 0.5 mW to minimize any laser-induced alterations of the sample. The scattered photons passed through the notch filter and grating in the monochromator to remove the Rayleigh scattering and were collected with a UV/visible sensitive liquid-nitrogen-cooled CCD detector (Horiba–Jobin Yvon CCD-3000V). The spectral resolution is ~1 cm⁻¹ for the spectra shown. The powder samples were loaded into an in situ cell (Linkam, TS1500) that allowed for sample treatments in oxidizing and reducing conditions. The oxidizing environment was created using a gas flow rate of 30 mL/min with an oxygen-to-helium percentage of 10%, while the reducing environment was created with a hydrogen-to-helium percentage of 5% at the same flow rate. Near-edge X-ray absorption fine structure (NEXAFS) measurements were performed at the U1A beamline at the National Synchrotron Light Source (NSLS) at Brookhaven National Labs. Specific details about the exact setup can be found in previous publications.¹⁷ NEXAFS measurements were taken as a function of incident X-ray photon energy for the vanadium and titanium L-edges and the oxygen K-edge, with a resolution of approximately 0.8 eV.

2.3. Photocatalysis. Photocatalytic studies were carried out using a diffuse reflectance infrared Fourier transform spectroscopy (DRIFTS) cell with a NEXUS 470 FTIR spectrometer equipped with a MCT detector. The DRIFTS cell is a Harrick Praying Mantis equipped with a high-temperature reaction chamber (Figure 2), which allows heating of the sample to 600 °C and evacuation down to 10⁻⁷ Torr. UV light was introduced to the sample through a fused silica fiber optic cable, which is attached to a 450W Thermo Oriel xenon arc lamp. A water filter was placed in between the fiber optic and the arc lamp to remove any IR radiation from the arc lamp. Two long-pass filters with cutoff wavelengths of 400 and 515 nm were used to modify the spectrum of the arc lamp and were inserted in front of the

TABLE 1: Chemical Composition, Pore Volume, and Band Gap Energy of ETS-10 and Vanadium-Incorporated ETVS-10

sample #	V/(V+Ti)	Si/(Ti+V)	(Na+K)/(Ti+V)	micropore volume (cm ³ /g)	band gap (eV)
1	0	4.49 ± 0.27	1.39 ± 0.25	0.157	4.32
2	0.11 ± 0.01	4.60 ± 0.14	1.53 ± 0.18	0.117	4.15
3	0.30 ± 0.02	2.39 ± 1.09	0.64 ± 0.31	0.135	3.66
4	0.41 ± 0.02	3.11 ± 0.26	0.72 ± 0.16	0.136	3.58
5	0.99 ± 0.01	5.23 ± 0.47	1.18 ± 0.32	0.129	3.81

water filter. All spectra were collected from 100 scans at a resolution of 4 cm⁻¹ and were obtained at a mirror velocity of 1.90 cm/s.

To determine if the vanadium-incorporated samples of ETS-10 have increased reactivity, the polymerization of ethylene was used as a model reaction.⁶ In this reactivity test, the following protocol was used. (1) The catalyst sample was dehydrated under vacuum for 1 day at 350 °C. This temperature was chosen because it allowed nearly complete removal of adsorbed water without causing any structural damage. (2) After dehydration, the sample was cooled to 25 °C, and a background spectrum was measured. (3) Ethylene was introduced into the cell up to a pressure of ~70 Torr and allowed to equilibrate for several minutes. (4) The UV lamp was turned on, and spectra were collected every 2 min for 6 h automatically with the spectrometer software. (5) At the end of 6 h, the lamp was turned off, and the cell was evacuated to remove any gaseous and physisorbed ethylene. (6) Finally, a spectrum was collected once all of the gaseous species had been evacuated.

To obtain a measure of the relative concentration of polyethylene in the samples, the area under the peaks associated with polyethylene were determined minus the area of the samples before polyethylene formation. This area was determined for all of the spectra throughout the 6 h period and then plotted as a function of time.

3. Results

3.1. Sample Characterization. Table 1 summarizes the elemental compositions of the five samples, as obtained from EDAX measurements, along with the micropore volume obtained from N₂ adsorption isotherms (t-plot method). The elemental compositions of the samples are in good agreement with the ideal unit cell, and there is little change in the fraction of V/(V+Ti) from that in the synthesis gel. The ratios of Si/(Ti+V) in samples 3 and 4 are low, but otherwise, the samples appear to be of good quality. These numbers indicate that the ratios are, perhaps, effected by the presence of a small amount of amorphous material or a small concentration of TiO₂ as an impurity. The same is true for the (Na+K)/(Ti+V) ratios that normally should be a factor of 2. However, these artifacts have been examined throughout this work and are shown not to alter the results presented here. The micropore volume of the vanadium samples are all close to the experimental value, 0.16 cm³/g for ETS-10, the only exception being the 0.13ETVS-10, which has a slightly lower value, probably due to the presence of a greater amount of quartz as an impurity in the sample compared to the other samples.

Figure 3 shows the X-ray diffraction patterns of the ETVS-10 samples, AM-6 and ETS-10. All samples show excellent crystallinity and contain no amorphous background and only small amounts of impurities such as quartz and TiO₂ (anatase), as indicated in the figure. The actual amount of TiO₂ was determined to be approximately 2% by weight in both the 0.33

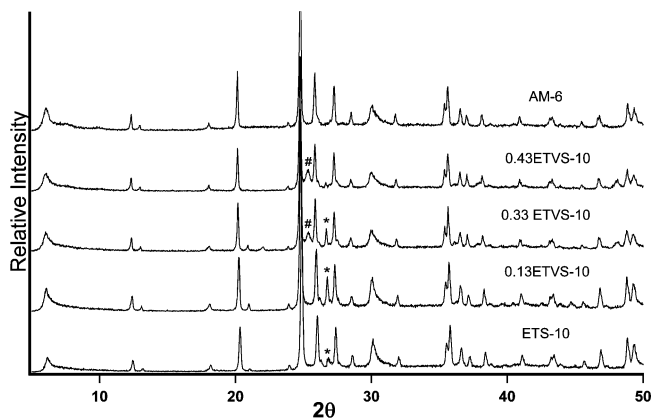


Figure 3. XRD patterns of ETS-10 and vanadium-substituted ETS-10. Small traces of anatase (#) and quartz (*) are visible in the vanadium-substituted ETS-10s.

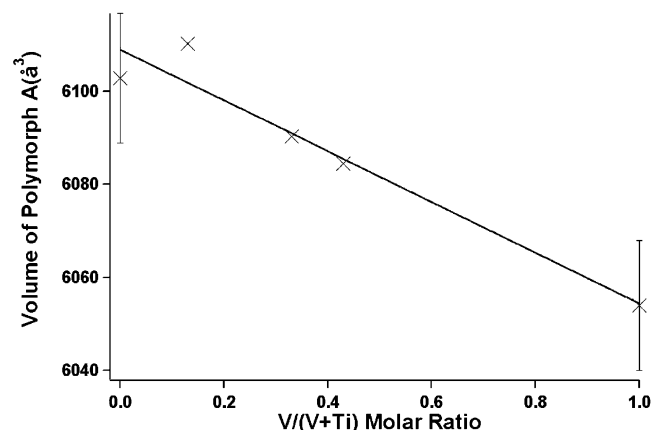


Figure 4. Volume change with isomorphous substitution of V for Ti in ETS-10 for polymorph A. A curve was fitted through the points only as a guide.

and 0.43ETVS-10. This value was obtained by comparing the relative intensity ratio of the TiO₂ peak at 25.32° 2θ to that of the 24.64° 2θ peak in ETS-10 of samples with known weight fractions of ETS-10 and TiO₂.

Using the XRD patterns and a least-squares refinement method,^{18,19} the volume of the unit cell (using the dimensions of polymorph A) was determined for each sample and plotted as a function of percent V in the sample (Figure 4). There is a systematic decrease in unit cell volume with the incorporation of vanadium for titanium in the chains of ETS-10. This is expected, as both vanadium(IV) and vanadium(V) in an octahedral coordination have smaller ionic radii (72 and 68 pm, respectively) than titanium(IV) in the same coordination environment (74.5 pm).²⁰ These results are also consistent with calculations on cluster models by Shough et al.,²¹ which predict this compression of the chains in the vanadium-incorporated structures.

The SEM images (Figure 5) show the crystal size and shape differences for the ETS-10, 0.43ETVS-10, and AM-6 samples that result from the different synthesis conditions. The ETS-10 sample is made up of small crystals, approximately 0.5 μm, which are square bipyramidal in shape. The 0.33 (not shown), 0.43ETVS-10, and AM-6 samples are larger in size and are mostly truncated bipyramidal in shape, with a different degree of development of the square and trapezoidal facets. There is also the appearance of crystals with a second morphology in the 0.43ETVS-10 samples, which could be the quartz or anatase impurities.

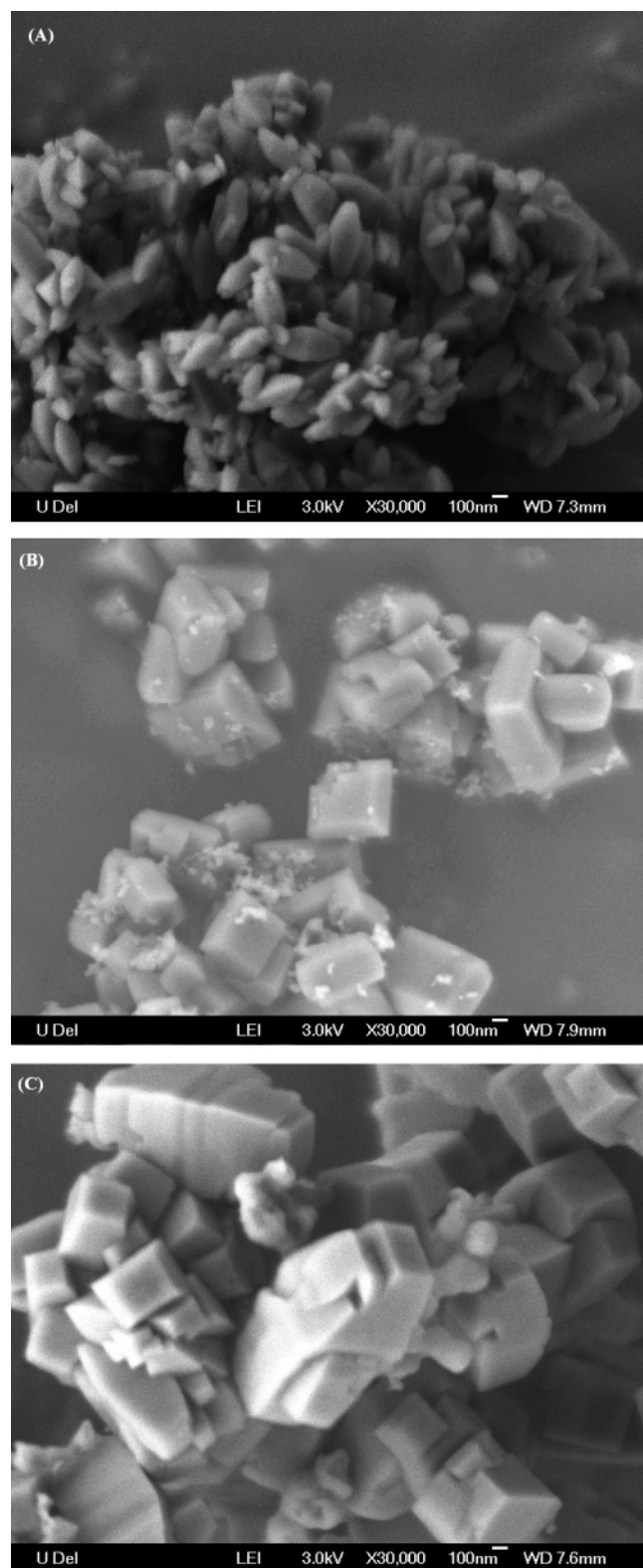


Figure 5. SEM of (A) ETS-10, (B) 0.43ETVS-10, and (C) AM-6.

The UV/vis spectra in Figure 6 show substantial differences between the ETVS-10 samples and ETS-10. First, in the ETS-10 sample, the UV/vis spectrum is dominated by a band gap absorption around 350 nm that corresponds to a charge transfer of the $O(2p) \rightarrow Ti(3d)$ transition,^{21,22} with no absorbance above 400 nm. In the ETVS-10 and AM-6 samples, this feature is blue shifted along with the appearance of three new absorbance features at 450, 594, and 850 nm. The absorbance at 450 nm is typical of a charge-transfer transition that occurs in octahedral

V^{5+} , while bands above 600 nm are typically associated with metal-to-metal transitions with V^{4+} .^{23–27} However, recent theoretical results suggest that the 594 nm peak is also a charge-transfer transition.²⁸ These results suggest that there are two different oxidation states for vanadium in the ETVS-10 and AM-6 samples.

The band gap energies of the five different samples (Table 1) were determined using the method of Gao and Wachs,²⁹ which was derived from the general power law of Davis and Mott³⁰

$$\alpha \hbar \omega \propto (\hbar \omega - E_g)^n$$

where α is the absorption coefficient, $\hbar \omega = h\nu$ is the photon energy, and $n = 2, 3, 1/2, 3/2$ for indirect allowed, indirect forbidden, direct allowed, and direct forbidden transitions, respectively. In this method, Gao and Wachs used an n value of 1/2 and determined the band gap energy from a plot of $[F(R_\infty)h\nu]^2$ versus $h\nu$, where $F(R_\infty)$ is Kubelka–Munk units and $h\nu$ is the incident photon energy. The value of n is usually determined by the best linear fit in the lower absorption region;^{31,32} however, several n values are usually good fits, and here, the value of 1/2 was used for all samples for consistency. Gao and Wachs have shown that, although values of E_g may change with the choice of n , similar trends will be observed for the samples. One should also consider that determining band gap energies for these materials with the absorbance spectra shown in Figure 6 is not straightforward since there are multiple absorbance features. Here, the band gap energies are calculated using the strong absorbance around 350 nm, even though there is clearly absorbance at larger wavelengths for the vanadium samples. Thus, for this reason, the band gap energies reported here should be viewed as upper limits, and here, there is the possibility of electron–hole formation at higher wavelengths/lower energies that correlate with these absorbance features in the vanadium-incorporated samples. This partly explains the higher value reported for ETS-10, 4.32 eV, compared to the previously reported value of 4.03 eV.³³ The other possible reason for the difference in values is that the ETS-10 sample in this study was synthesized from a P-25 titanium source, and that in reference 33 was obtained from $TiCl_3$. There are several papers^{16,34} that support this hypothesis, suggesting that ETS-10 synthesized from P-25 shows better crystallinity than those from other titanium sources.

With the incorporation of the vanadium, there was a steady decrease in the band gap energy from the ETS-10 value of 4.32 eV down to 3.58 eV for 0.43ETVS-10, followed by a small increase for the AM-6 sample at 3.81 eV. These values for the band gap approach the values that we found for TiO_2 (anatase) and P-25 using the same methods, which were 3.38 eV (3.18 eV for $n = 2$) and 3.49 eV (3.04 eV for $n = 2$). However, since some of the ETVS-10 samples contained approximately 2% anatase, a mixture of pure ETS-10 and anatase was used to confirm that the band gap energies were not effected by this impurity. The results from this experiment confirm that the band gap values were identical to those determined before. Thus, this change in the band gap energy allows lower energy photons to excite electron–hole pairs, which then can react with adsorbed molecules. On the other hand, the vanadium atoms can also act as electron/hole traps that may promote charge carrier recombination and decrease the photoactivity.³⁵

The Raman spectra (Figure 7a) present clear evidence for the isomorphous substitution of V for Ti in the ETVS-10 and AM-6 samples. In Figure 7a, one observes the characteristic $-Ti-O-Ti-$ bond vibration along the chain at 727 cm^{-1} , which decreases with increasing V content, while a new band

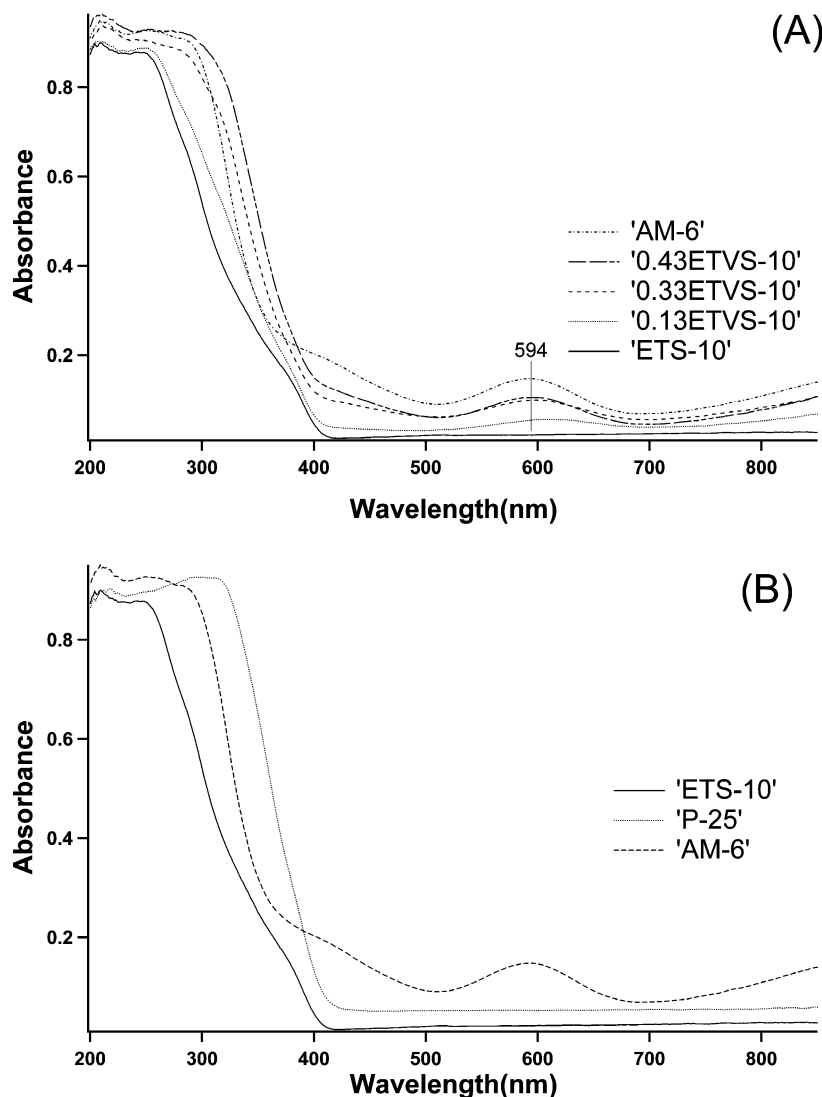


Figure 6. (A) UV/vis spectra of ETS-10 and vanadium-substituted ETS-10. (B) UV/vis spectra of ETS-10, AM-6, and P-25.

appears at 867 cm^{-1} associated with the -V-O-V- stretch.^{13,36} Also, the presence of a band in between these two, at 839 cm^{-1} , appears for the higher content ETVS-10 samples and is tentatively assigned to a -V-O-Ti- associated vibration. All other peaks in the ETVS-10 and AM-6 samples are seen in ETS-10 except those assigned to anatase impurities at 514 and 395 cm^{-1} .

The presence of vanadium also creates new surface sites at the termination of the chains or at defects along the chain that expose the vanadiol group. These new surface sites along with other surface species can be seen in the FTIR spectra of the dehydrated ETVS-10s and AM-6 samples (Figure 7b). All three samples show the characteristic stretch of the SiO-H at 3734 cm^{-1} associated with the SiOH stretching vibration at the external surface of the crystals.³⁷ The signal at 3716 cm^{-1} assigned to the TiO-H stretch is observed in ETS-10 and, to a lesser extent, in the 0.33ETVS-10. The presence of a new band at 3703 cm^{-1} in the vanadium samples is tentatively assigned to the VO-H stretch; however, further research is needed to confirm this since the ETS-10 sample also shows a small absorbance (as a shoulder) in this region (although this is believed to be caused by defects). Since these spectra are not normalized, there appears to be a higher concentration of OH sites for the ETVS-10 samples compared to the V-containing samples, perhaps suggesting a higher number of defects for the

ETS-10 sample. Along with these surface sites, the presence of residual water can also be observed in the FTIR spectrum with bands appearing at 3666 , 3572 , and 3493 cm^{-1} . This residual water is difficult to remove, as others have observed.^{6,37}

Vanadium has several oxidation states,²⁰ and there has been some uncertainty in the literature as to the oxidation state of vanadium in vanadium-incorporated samples. Rocha et al.^{13,14} were unable to observe any evidence for V^{5+} in AM-6 or any of the ETVS-10 samples, and only an EPR signal assignment for V^{4+} was reported. NEXAFS measurements were undertaken to determine the oxidation state of vanadium in the ETVS-10 and AM-6 samples. In Figure 8a, one can observe that the O K-edge feature dominates the NEXAFS spectrum in the $500\text{--}600\text{ eV}$ range and that the V L-edge peaks at $510\text{--}530\text{ eV}$ grow with increasing vanadium content.³⁸ The values for peaks here are about 0.5 eV higher than those in reference 38 due to lack of calibration of the scale for the incident energy. In the AM-6 sample, the V L-Edge has the best resolution, and the presence of two peaks corresponding to the L_{III} - and L_{II} -edges of V^{5+} are clearly visible.³⁸ These two peaks also possess low-energy shoulders that match up with the position of L_{III} - and L_{II} -edges for V^{4+} . The ETVS-10 samples also show similar peaks, though, due to increased noise, it is difficult to resolve them. Thus, the presence of both V^{4+} and V^{5+} can be seen from the NEXAFS data of the ETVS-10 and AM-6 samples. To estimate the relative

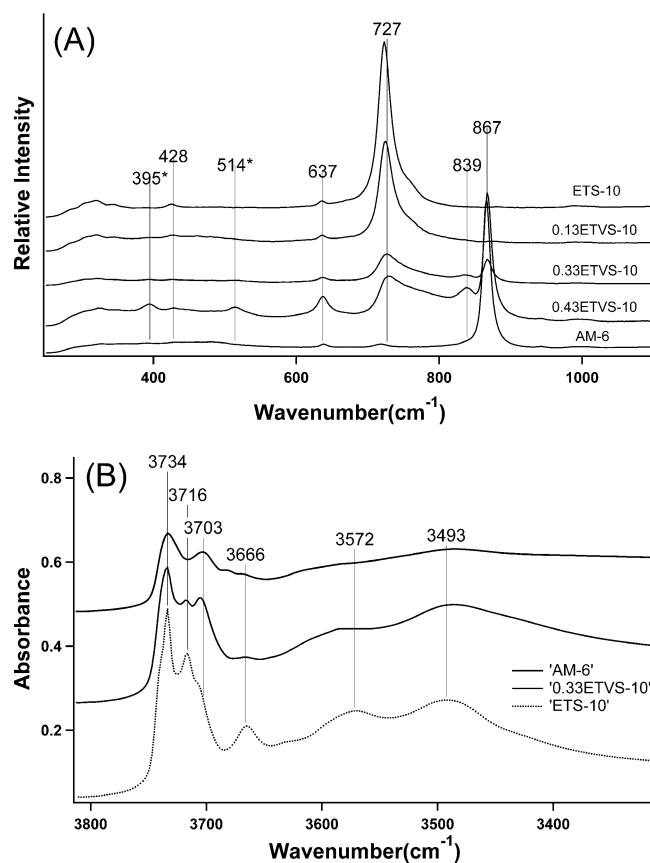


Figure 7. (A) Raman spectra of ETS-10, AM-6, and ETVS-10s, along with TiO₂ impurities (*), (B) FTIR of surface sites on ETS-10, ETVS-10s, and AM-6.

concentration of the two oxidation states, Gaussian curves were fitted to the peaks (AM-6), and the ratios of the V⁴⁺ peak area to total V⁴⁺ and V⁵⁺ peak area for the L_{III}- and L_{II}-edges was determined. These ratios indicate that 20–40% of V is in the 4+ oxidation state in AM-6.

To test the structural stability of the different vanadium samples, Raman spectra were collected under reducing (H₂) and oxidizing (O₂) conditions at 450 °C for 2 h to determine if the overall structure remained intact. The AM-6, 0.33ETVS-10, and 0.43ETVS-10 samples showed little change in the characteristic –V–O–V– stretch at 867 cm⁻¹ (not shown) under H₂, indicating that the structure is stable under reducing conditions. However, the result is quite different under oxidizing conditions (Figure 8b) where the 0.33 and 0.43ETVS-10 samples retain most of their structural stability but where AM-6 completely loses the characteristic stretch at 867 cm⁻¹. These results have been confirmed by XRD measurements (not shown) that show the loss of the structure for AM-6 upon oxidation. There is also the formation of a band at 936 cm⁻¹ which has tentatively been attributed to a V=O bond at defects sites.¹³ However, V=O bonds usually occur at higher frequencies, and recent theoretical results by Magg et al.³⁹ suggest that this is a V–O–Si bond. This loss in structural stability could be caused by the oxidation of the V^{IV} to V^V in the chain causing the collapse of the ETS-10 structure. This theory is supported by energy calculations by Shough et al.²¹ in which they predict that a chain of –V^V–O–V^V– is energetically unfavorable.

3.2. Photocatalysis. The polymerization of ethylene was used as a test reaction to determine the photoreactivity of the ETVS-10 and AM-6 samples since it has been shown to be a simple reaction, easily quantifiable by IR spectroscopy.⁶ Figure 9a

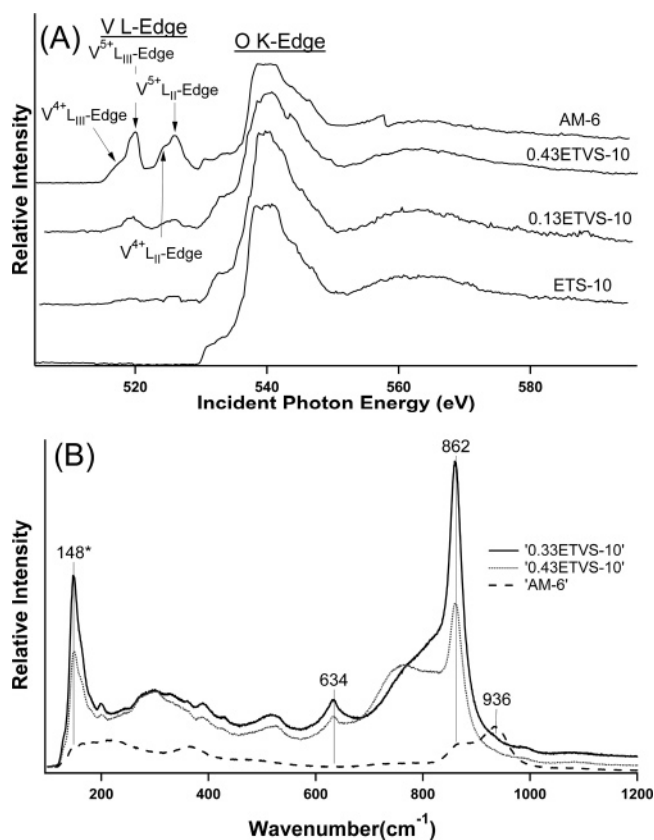


Figure 8. (A) NEXAFS of V L-Edge features and O K-Edge features. (B) Raman of AM-6, 0.33ETVS-10, and 0.43ETVS-10 in O₂ at 450 °C for 2 h, along with TiO₂ impurities (*).

shows the changes to the C–H stretching region observed during this reaction using UV/vis light (200–800 nm), in which the formation of the saturated polyethylene bonds is confirmed by the bands at 2924 and 2854 cm⁻¹. Also observed in the spectra is the gaseous ethylene stretch at 2987 cm⁻¹ and the physisorbed ethylene stretches at 3248, 3084, and 2966 cm⁻¹, subsequently removed upon evacuation.

By determining the area under both the 2924 and 2854 cm⁻¹ peaks of polyethylene for each spectrum throughout the 6 h of photoreaction and subtracting the initial area at time zero, the formation of polyethylene can be compared as a function of time, as in Figure 9b. In this figure, the peak area is plotted as a function of time for the ETS-10, 0.43ETVS-10, 0.33ETVS-10, AM-6, and P-25 samples; 0.43ETVS-10 is the most active.

For this reaction, the rate of formation is dependent on the adsorption effects of the materials, the ability of the material to create electron–hole pairs, and the relative amount of defects in the sample. In regard to the adsorption effects, all samples have similar pore size and show adsorption of ethylene; however, the amount of ethylene adsorbed cannot be quantified from the FTIR data, and crystal size may have an effect on the total amount of ethylene adsorbed. However, since the difference in crystal size between the samples is small, this effect is expected to be minimal. As for the ability of the material to create electron–hole pairs, the vanadium-incorporated samples have been shown to have lower band gap energies along with increased absorbance in the low-energy region of the UV/vis spectra, and thus, the vanadium-containing samples are expected to generate more electron–hole pairs. Also, the intensity of the UV/vis radiation that exits the fiber optic cable will greatly affect the rate of formation of electron–hole pairs, and thus, every effort was made to keep the UV/vis radiation constant through-

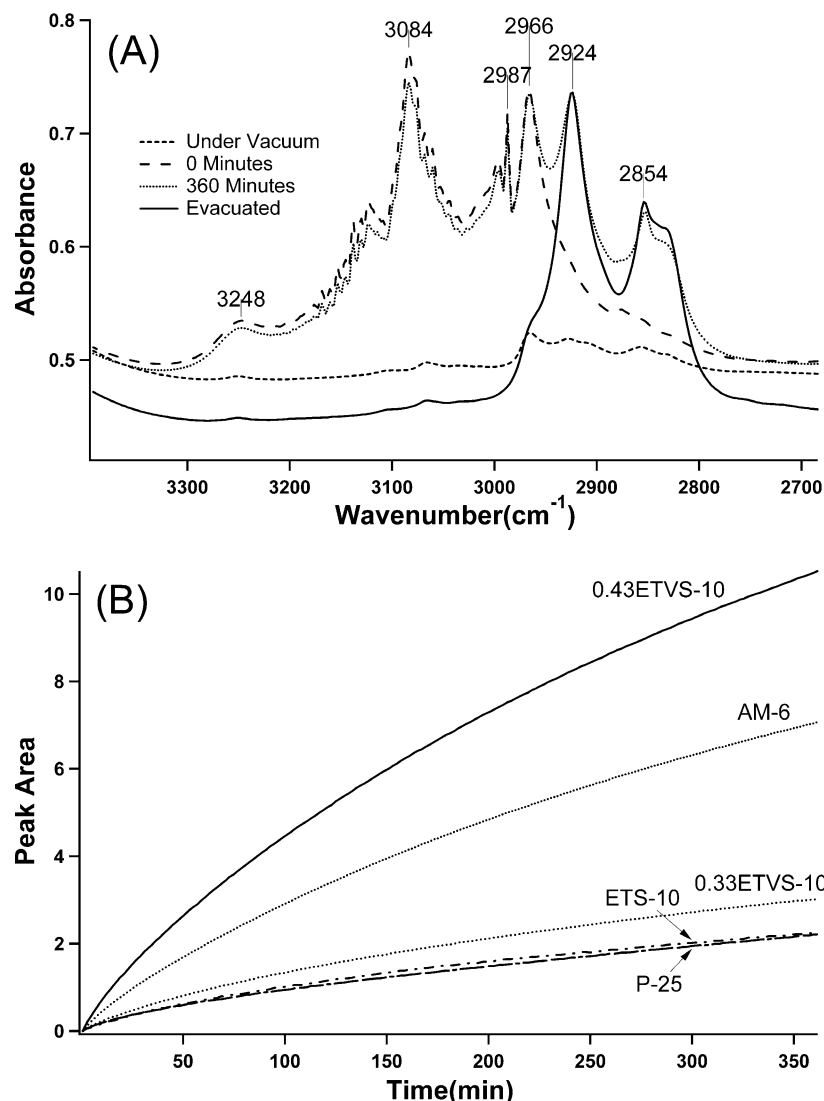


Figure 9. (A) Reaction of ethylene on 0.43ETVS-10. (B) Peak area of polyethylene versus reaction time for ETS-10, 0.43ETVS-10, 0.33ETVS-10, AM-6, and P-25 samples with no filter.

out each experiment; however, there is some small inherent experimental error in this process. As for defects in the sample, at this time, it is not possible to quantify the amount of defects from the FTIR data, and this will add some error to the process.

To determine if the absorbance around 450 nm in the ETVS-10 and AM-6 samples is photocatalytically active, a 400 nm filter was placed before the water filter on the UV lamp to filter out any radiation with a shorter wavelength. Figure 10a shows that both AM-6 and 0.43ETVS-10, under visible light (400–800 nm), are active, but their activity is lower than that of P-25, which has a small absorbance above 400 nm. Reasons for the higher activity could be based on the fact that P-25 has more charge-transfer sites for electron–hole pairs than the ETS-10 structure. A 515 nm filter (wavelength range, 515–800 nm) was used to test whether the 594 nm metal–metal transition could be used for photocatalysis and compared to the results obtained from the 400 nm filter and no filter cases. On the basis of Figure 10b, which shows the difference spectra for the AM-6 samples before and after reaction for the three cases, there appears to be no reaction induced by light at or above 515 nm for the AM-6 sample, the tiny peaks on the 515 nm case being the effects of stray light.

4. Discussion

In ETS-10, an electron–hole pair is free to travel down the chain and react with ethylene at either a defect site along the chain or at the ends of the chain. Thus, the structure of the titanium chains plays an important role in the reactivity of ETS-10 and determines if an electron–hole pair will react with an absorbed molecule or recombine along the chain. Howe et al.⁶ have used Raman measurements to determine the relative amount of defects in two different ETS-10 samples, along with EPR measurements to show that these differences lead to differences in the relaxation mechanisms for the electron–hole pairs. They demonstrated that only the more defective ETS-10 sample would form superoxide ions and reduced titanium when irradiated in the presence of oxygen and ethylene, respectively, while the less defective sample showed no EPR signal in either environment.

In this study, we have changed the local environment of the titanium chains by the addition of vanadium, which leads to clear differences in both the Raman and UV/vis spectra. The effects in local structure are the decrease in the intensity of the –Ti–O–Ti– Raman stretch and the increase in the intensity of the –V–O–V– stretch with increasing vanadium content. For the intermediate concentrations of vanadium, we observed

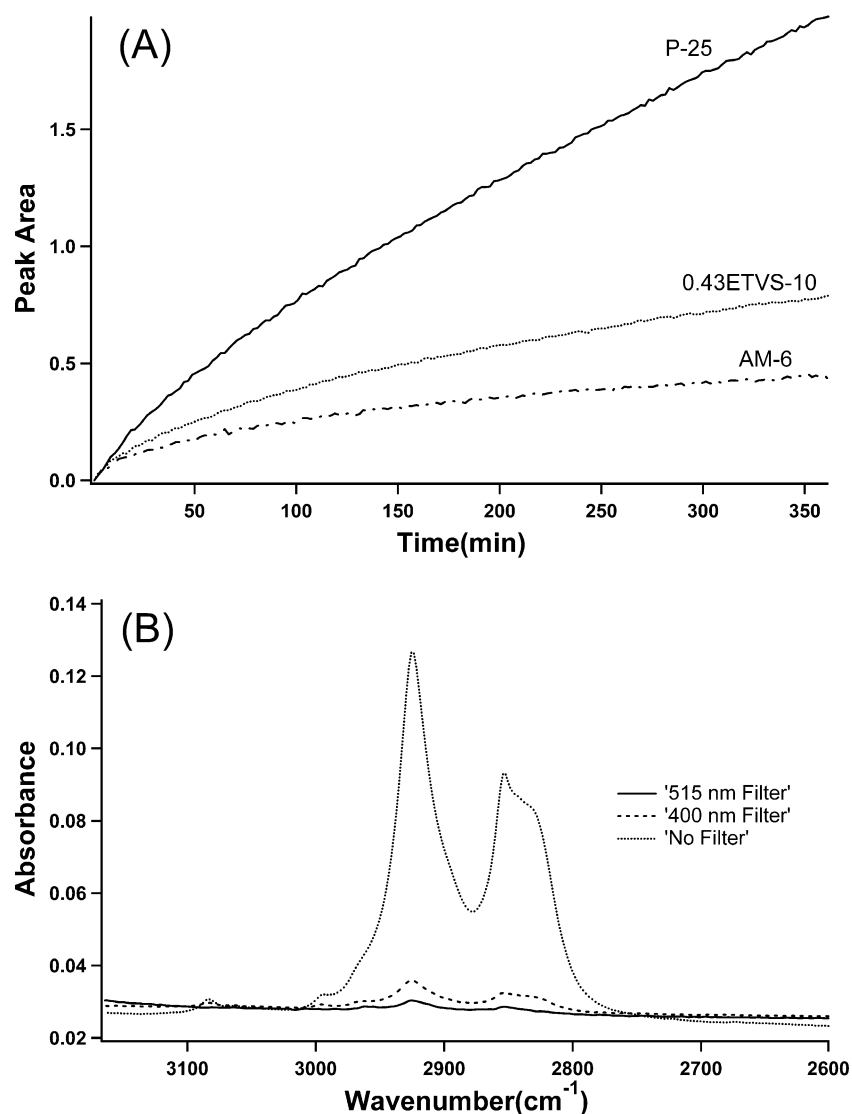


Figure 10. (A) Peak area of polyethylene versus reaction time for 0.43ETVS-10, AM-6, and P-25 samples with a 400 nm filter. (B) Difference IR spectra before and after reaction for AM-6 with no filter, a 400 nm filter, and a 515 nm filter.

the formation of a broad $-\text{Ti}-\text{O}-\text{V}-$ Raman peak. This peak along with the $-\text{V}-\text{O}-\text{V}-$ peak were not observed by Brandao et al.,¹⁴ suggesting that their samples had little or no vanadium in the chains and that the broadening they observed was perhaps due to defects along the chain. The width of these peaks also helps describe the structural order of the chains, where the 727 cm^{-1} peak in ETS-10 and 0.13ETVS-10 is relatively narrow (fwhm of 22 and 25 cm^{-1} , respectively) compared to that of the 0.33ETVS-10 sample (fwhm of 51 cm^{-1}) and the 0.43ETVS-10 sample, where the presence of the $-\text{Ti}-\text{O}-\text{V}-$ peak makes unfeasible the measurement of a fwhm. These differences in the spectra suggest a structure for the intermediate vanadium-incorporated samples that is relatively disordered along the chain. This assessment is in agreement with the theoretically calculated results of vibrational frequencies for ETS-10 obtained by Damin et al.⁴⁰ These authors attribute the Raman peak at 727 cm^{-1} to an out-of-phase stretch of the two apical oxygen atoms on the titanium octahedron. Their models showed that this stretch was split by coupling with a symmetric stretch involving the $-\text{Si}-\text{O}-\text{Si}-$ atoms in the three-membered ring around the chain, resulting in two stretches at 758 and 726 cm^{-1} . The authors assigned the 758 cm^{-1} stretch to an asymmetric coupling with the $-\text{Si}-\text{O}-\text{Si}-$ stretch and the 726 cm^{-1} stretch to a symmetric coupling. These two modes are in good

agreement with the experimental Raman peak at 727 cm^{-1} and its high-frequency tail, which they argued was made up of the stronger intensity, symmetrically coupled stretch and the lower intensity, asymmetrically coupled stretch. These results suggest the incorporation of vanadium is increasing the asymmetric coupling and decreasing the symmetric coupling since the 727 cm^{-1} peak decreases in intensity and broadens as more vanadium is added to the samples. This may be a result of the asymmetric nature of the chains once vanadium is added, hence, changing the local environment of the chains and creating strain on the overall structure. This complex picture of the bonding structure along the titanium and vanadium chains for the different samples is in agreement with the recently calculated results from Shough et al.²¹ for cluster models containing varied amounts of vanadium.

Vanadium incorporation also causes a shift in the band gap energy, as seen in the UV/vis spectra and Table 1, along with an increase in absorbance in the 450 nm region and possible metal-to-metal transitions for vanadium appearing at 594 and 850 nm. The more disordered samples, 0.33ETVS-10 and 0.43ETVS-10, interestingly have the lowest band gap, while AM-6, with more vanadium, has a higher band gap energy. This suggests that the disordered bond structure along the chain has a strong influence on the band gap energy of the sample.

The photoreactivity studies indicate several properties of the UV/vis transitions, along with the overall reactivity of these materials. There is a significant decrease in the overall reactivity of the samples when the filters are placed on the UV lamp (Figure 10b), which is due to the overall decrease in the photon flux with the filters on. The transition at 594 nm⁻¹ for the vanadium samples shows no reactivity (Figure 10b), suggesting that this is a localized transition that does not lead to charge separation. Even though the AM-6 sample has the largest absorbance at around 450 nm, it is the 0.43ETVS-10 sample that shows the greatest reactivity with the 400 nm filter. This suggests that, beyond some optimal concentration, the vanadium atoms start acting as recombination centers and thus decrease the overall reactivity of the sample. This hypothesis is supported by the calculations of Shough et al.²¹ in which they showed that the V^V sites along the chain act as electron traps and the V^{IV} sites act as hole traps. They also established that, at low concentrations of vanadium, the two different oxidation states would be separated, thus increasing charge separation. However, they also suggested that, at high concentrations, the two oxidation states of vanadium would be close enough that they would begin promoting recombination and thus decrease the sample's photoreactivity.

5. Conclusions

ETS-10, AM-6, and ETVS-10 have been synthesized to create samples with varying amounts of vanadium incorporated into the ETS-10 framework structure. The chemical composition has been verified with EDAX, and the V/(V+Ti) ratio is consistent with the chemical compositions in the parent synthesis gel solutions. The ETS-10 structure has been confirmed in the samples with XRD, N₂ adsorption, and SEM images and are consistent with previously reported results.^{2,13,14}

Raman spectra provide evidence for vanadium in octahedral coordination along the chain with the decrease of the -Ti-O-Ti- peak and the formation of the -V-O-V- peak. The presence of a peak at 837 cm⁻¹ for the intermediate samples was also observed and assigned to a -Ti-O-V- bond. Also, a new surface site assigned to the VO-H stretch at 3703 cm⁻¹ was seen in the infrared spectrum and increased in intensity with increasing vanadium content.

The presence of both V(IV) and V(V) has been observed in the NEXAFS spectrum in the vanadium L-edge region. Both the L_{III} and L_{II} peaks for vanadium(V) have low-energy shoulders which correspond to the vanadium(IV) L_{III} and L_{II} peaks.

The incorporation of vanadium into the ETS-10 structure decreases the band gap from 4.32 to 3.58 eV, which is close to the value of 3.38 eV determined with the same methods for anatase. This lowering of the band gap and the absorbance features in the low-energy region of the UV/vis spectra has led to increased photoreactivity in the visible region, along with an overall increase in photocatalytic activity.

Acknowledgment. We thank J. Rabolt for the use of Raman equipment, J. G. Chen for his help with and analysis of the NEXAFS data, C. Ni and F. Kriss for help with the SEM images, and Anne-Marie Shough for her thoughtful discussions and insights on the vanadium samples. We also want to thank the two anonymous reviewers for helpful comments. Funding for this research was provided by the U.S. Department of Energy under Grant No. DE-FG02-99ER14998.

Supporting Information Available: XRD patterns of AM-6 after dehydration and reaction with ethylene and after oxidation

in O₂ for 2 h at 400 °C. This material is available free of charge via the Internet at <http://pubs.acs.org>.

References and Notes

- (1) Kuznicki, S. M. U.S. Patent 4,853,202, 1989.
- (2) Anderson, M. W.; Terasaki, O.; Ohsuna, T.; Philippou, A.; Mackay, S. P.; Ferreira, A.; Rocha, J.; Lidin, S. *Nature* **1994**, *367*, 347.
- (3) Lin, Z.; Rocha, J.; Navajas, A.; Tellez, C.; Coronas, J. Q.; Santamaria, J. *Microporous Mesoporous Mater.* **2004**, *67*, 79.
- (4) Zecchina, A.; Xamena, F. X. L. I.; Paze, C.; Palomino, G. T.; Bordiga, S.; Arean, C. O. *Phys. Chem. Chem. Phys.* **2001**, *3*, 1228.
- (5) Robert, R.; Rajamohanam, P. R.; Hegde, S. G.; Chandwadkar, A. J.; Ratnasamy, P. *J. Catal.* **1995**, *155*, 345.
- (6) Krishnandi, Y. K.; Southon, P. D.; Adesina, A. A.; Howe, R. F. *Int. J. Photoenergy* **2003**, *5*, 131.
- (7) Xamena, F. X. L. I.; Calza, P.; Lamberti, C.; Prestipino, C.; Damin, A.; Bordiga, S.; Pelizzetti, E.; Zecchina, A. *J. Am. Chem. Soc.* **2003**, *125*, 2264.
- (8) Calza, P.; Paze, C.; Pelizzetti, E.; Zecchina, A. *Chem. Commun.* **2001**, 2130.
- (9) Borello, E.; Lamberti, C.; Bordiga, S.; Zecchina, A.; Arean, C. O. *Appl. Phys. Lett.* **1997**, *71*, 2319.
- (10) Linsebigler, A. L.; Lu, G. Q.; Yates, J. T. *Chem. Rev.* **1995**, *95*, 735.
- (11) Brandao, P.; Philippou, A.; Valente, A.; Rocha, J.; Anderson, M. *Phys. Chem. Chem. Phys.* **2001**, *3*, 1773.
- (12) Lazar, K.; Das, T. K.; Chaudhari, K.; Chandwadkar, A. J. *Porous Mater. Environ. Friendly Processes, Proc. Int. FEZA Conf.* **1999**, *125*, 301.
- (13) Rocha, J.; Brandao, P.; Lin, Z.; Anderson, M. W.; Alfredsson, V.; Terasaki, O. *Angew. Chem., Int. Ed.* **1997**, *36*, 100.
- (14) Brandao, P.; Valente, A. A.; Rocha, J.; Anderson, M. W. Impact of Zeolites and Other Porous Materials on the New Technologies at the Beginning of the New Millennium, Parts A and B. *Stud. Surf. Sci. Catal.* **2002**, *142*, 327.
- (15) Uma, S.; Rodrigues, S.; Martyanov, I. N.; Klabunde, K. J. *Microporous Mesoporous Mater.* **2004**, *67*, 181.
- (16) Lv, L.; Su, F. B.; Zhao, X. S. *Microporous Mesoporous Mater.* **2004**, *76*, 113.
- (17) Lusvardi, V. S.; Barteau, M. A.; Chen, J. G.; Eng, J.; Fruhberger, B.; Teplyakov, A. *Surf. Sci.* **1998**, *397*, 237.
- (18) Bish, D. L.; Post, J. E. *Modern Powder Diffraction; The Mineralogical Society of America: Washington, DC, 1989; Vol. 20.*
- (19) Laugier, J.; Bochu, B. *CELREF*, 3 ed.; LMGP: Grenoble, France, 2003.
- (20) Winter, M. Webelements. <http://www.webelements.com/>, 1993.
- (21) Shough, A. M.; Doren, D. J.; Lobo, R. F.; Nash, M. J. *J. Phys. Chem. C* **2007**, *111*, 1776.
- (22) Zimmerman, A. M.; Doren, D. J.; Lobo, R. F. *J. Phys. Chem. B* **2006**, *110*, 8959.
- (23) Catana, G.; Rao, R. R.; Weckhuysen, B. M.; Van Der Voort, P.; Vansant, E.; Schoonheydt, R. A. *J. Phys. Chem. B* **1998**, *102*, 8005.
- (24) Luan, Z. H.; Xu, J.; He, H. Y.; Klinowski, J.; Kevan, L. *J. Phys. Chem.* **1996**, *100*, 19595.
- (25) Dzwigaj, S.; Massiani, P.; Davidson, A.; Che, M. *J. Mol. Catal. A: Chem.* **2000**, *155*, 169.
- (26) Baltes, M.; Cassiers, K.; Van Der Voort, P.; Weckhuysen, B. M.; Schoonheydt, R. A.; Vansant, E. F. *J. Catal.* **2001**, *197*, 160.
- (27) Frunza, L.; Van Der Voort, P.; Vansant, E. F.; Schoonheydt, R. A.; Weckhuysen, B. M. *Microporous Mesoporous Mater.* **2000**, *39*, 493.
- (28) Shough, A. M.; Doren, D. J.; Lobo, R. F.; Nash, M. J. **2007**, in preparation.
- (29) Gao, X. T.; Wachs, I. E. *J. Phys. Chem. B* **2000**, *104*, 1261.
- (30) Davis, E. A.; Mott, N. F. *Philos. Mag.* **1970**, *22*, 903.
- (31) Hossein, A. A.; Hogarth, C. A.; Beynon, J. *J. Mater. Sci. Lett.* **1994**, *13*, 1144.
- (32) Khan, G. A.; Hogarth, C. A. *J. Mater. Sci.* **1991**, *26*, 412.
- (33) Lamberti, C. *Microporous Mesoporous Mater.* **1999**, *30*, 155.
- (34) Su, L. L. F.; Zhao, X. S. *J. Porous Mater.* **2006**, *13*, 263.
- (35) Martin, S. T.; Morrison, C. L.; Hoffmann, M. R. *J. Phys. Chem.* **1994**, *98*, 13695.
- (36) Su, Y.; Balmer, M. L.; Bunker, B. C. *J. Phys. Chem. B* **2000**, *104*, 8160.
- (37) Southon, P. D.; Howe, R. F. *Chem. Mater.* **2002**, *14*, 4209.
- (38) Kim, C. M.; Devries, B. D.; Fruhberger, B.; Chen, J. G. *Surf. Sci.* **1995**, *327*, 81.
- (39) Magg, N.; Immaraporn, B.; Giorgi, J. B.; Schroeder, T.; Baumer, M.; Dobler, J.; Wu, Z. L.; Kondratenko, E.; Cherian, M.; Baerns, M.; Stair, P. C.; Sauer, J.; Freund, H. J. *J. Catal.* **2004**, *226*, 88.
- (40) Damin, A.; Xamena, F. X. L.; Lamberti, C.; Civalieri, B.; Zicovich-Wilson, C. M.; Zecchina, A. *J. Phys. Chem. B* **2004**, *108*, 1328.